Mesopore Structure of Microcrystalline Cellulose Tablets Characterized by Nitrogen Adsorption and SEM: The Influence on Water-Induced Ionic Conduction

Martin Nilsson,[†] Albert Mihranyan,[†,‡] Sima Valizadeh,[†] and Maria Strømme*[,†]

Department of Engineering Sciences, The Ångström Laboratory, Uppsala University, Box 534, SE-751 21 Uppsala, Sweden, and Department of Pharmacy, Uppsala Biomedical Center, Uppsala University, Box 580, SE-751 23 Uppsala, Sweden

Received: October 13, 2005; In Final Form: April 14, 2006

Tablets of microcrystalline cellulose were formed at different compaction pressures and physical properties, such as pore size distribution, surface area, and pore surface fractality, were extracted from N_2 adsorption isotherms. These properties were compared to previously published data on the water-induced ionic conductivity of the tablets. The conduction process was shown to follow a percolation model with a percolation exponent of 2 and a porosity percolation threshold of ∼0.1. The critical pore diameter for facilitated charge transport was shown to be in the 5−20 nm range. When the network of pores with a diameter in this interval is reduced to the point where it no longer forms a continuous passageway throughout the compact, the conduction process is dominated by charge transport on the surfaces of individual microfibrils mainly situated in the bulk of fibril aggregates. A fractal analysis of nitrogen adsorption isotherms showed that the dominant interface forces during adsorption is attributed to surface tensions between the gas and the adsorbed liquid phase. The extracted fractal dimension of the analyzed pore surfaces remained unaffected by the densification process at low compaction pressures (<∼200 MPa). At increased densification, however, pore-surface structures smaller than ∼100 nm become smoother as the fractal dimension decreases from ∼2.5 at high porosities to ∼2.3 for the densest tablets under study.

Introduction

Cellulose is the most abundant biopolymers on Earth; more than 1000 billion metric tons of cellulose is annually being cultivated. Because of its enormous industrial importance, the cellulose molecule has been extensively studied. However, even if the chemical structure of this molecule is well-known, the physiochemical parameters governing its interactions with various solids and liquids are not fully understood.

Microcrystalline grades of cellulose (MCC) are the most frequently used excipients for direct compaction of tablets within the pharmaceutical industry. When cellulose is used for hosting and delivering drugs to the human body, its interactions with water becomes of uttermost importance. Upon contact with water, polar drug molecules ionize and get surrounded by a hydration shell consisting purely of water molecules. Even though this shell is dynamic, an exchange of water molecules between the shell and its surroundings continuously takes place. The lifetime for a bond between such ions and water is about 2 orders of magnitude larger than that for a bond between two water molecules.[1] Thus, when the pharmaceutical excipient cellulose absorbs water in the gastrointestinal tract, water molecules will surround the incorporated drug during the entire drug release process. It has earlier been indicated that the interactions between the free hydroxyl groups of the cellulose with the water molecules in the hydration shell regulate the speed by which the drug ions are able to leave the cellulose particles.[2] These interactions, and the charge transport properties of the constituent ions of water (OH^- and H_3O^+) in cellulose, are therefore important to analyze and understand in order to identify how the cellulose nanostructure should be modified to tailor the drug release process.

The individual cellulose chains tend to hydrogen bond strongly to neighboring chains and form cellulose microfibrils consisting of ∼8 × 8 chains in the wood pulp cellulose type made to produce MCC.[3] The lateral dimension of these microfibrils are ∼4 nm × 4 nm and they consist of crystalline interior regions and disordered surface regions.[4,5] Approximately 44% of the individual chains are thus located on the microfibril surfaces, resulting in an MCC crystallinity of ∼56% in accordance with transmission IR spectroscopy. The microfibrils form fibril aggregates, which in their turn form the cellulose particles.

In earlier work of ours,[6,7] we have presented that the charge transport mechanism in humid MCC may be governed by two parallel processes: one involving water constituent ions diffusing between adjacent lowest energy sites in disordered regions of the cellulose and the other caused by impurity ions, such as Na^+, and protons or H_3O^+ ions jumping between neighboring cellulose OH^- groups to which a primary water molecule is attached. At relative humidities of ∼37% (representing monolayer coverage of water on available sites in the cellulose) and higher, the latter process is totally dominating the charge transport.[7] This is also the process that has been in focus by cellulose researchers during the last half-century, see, e.g., Murphy,[8] Pethig,[9] Sapieha et al.,[10] Simula and Niskanen,[11] and references therein.

The aim of the present study is to investigate how densification influences physicochemical properties of the microcrystalline cellulose pore structure and how these properties, in their turn, affect the water-induced charge transport.

* Corresponding author. E-mail: maria.stromme@angstrom.uu.se.
[†] Department of Engineering Sciences, The Ångström Laboratory.
[‡] Department of Pharmacy, Uppsala Biomedical Center.

10.1021/jp055858v CCC: $33.50
Published on Web 07/22/2006

TABLE 1: Compaction Data of MCC Tablets[a]

tablet batch	compaction pressure [MPa]	tablet density [g/cm^3]
1	57.7 ± 0.5	1.01 ± 0.01
2	150.3 ± 2.5	1.15 ± 0.02
3	206.5 ± 1.4	1.25 ± 0.01
4	249.8 ± 2.1	1.31 ± 0.01
5	404.0 ± 1.8	1.39 ± 0.01

[a] The values are given as average value over 4 measurements ± standard deviation.

Materials and Methods

Materials. Microcrystalline cellulose (MCC, Avicel PH 101, FMC, Ireland) powder was used as delivered. Five batches of MCC tablets were produced. The tablets were compacted at pressures ranging from ~50 to ~400 MPa using an instrumented single punch press (Korch EK 0, Germany) equipped with 11.3 mm diameter punches. The tablet weight was varied between 210 and 300 mg in order to produce tablets of ~2.0 mm height. Prior to and after compaction, the powder and tablets, respectively, were stored over a saturated NaI solution, producing a relative humidity (RH) of ~37% corresponding to an MCC moisture content of ~4 wt %.[7] The apparent densities were calculated as the ratio between the sample weight at 37% RH and volume. Tablet data are summarized in Table 1.

Methods. *Nitrogen Adsorption.* Nitrogen adsorption isotherms at 77 K were recorded with an accelerated surface area and porosimetry analyzer (ASAP 2010, Micromeritics, USA). The tablets were degassed for ~8 h at a pressure of 2.66×10^{-3} Pa at 343 K prior to the adsorption measurements. This degassing procedure, which includes both application of heat and vacuum, ensures removal of water and any other gas and/or volatile contaminant from the sample. The satisfactoriness of the applied pretreatment to remove water present in MCC has previously been supported.[12,13] The tablet surface area and the distribution of pore volume (accessible to nitrogen) were calculated using the ASAP 2010 software, implementing the BET[14] and the BJH[15] methods, respectively.

The interpretation of adsorption isotherms for fractal surfaces has been a controversial problem for almost two decades, and several methods based on gas adsorption/desorption exist. Analysis of the initial layer-by-layer adsorption may in some cases be favorable,[16] while for other situations, using the capillary condensation part of the isotherm may give the most adequate results.[17] Fractal capillary condensation analysis of water adsorption/desorption isotherms has previously proven successful for obtaining information about the distribution of sites, both inside open pores and inside amorphous bulk regions, available to water molecules in various cellulose powder structures.[18] In the present work, we perform a similar analysis of nitrogen adsorption isotherms in order to acquire knowledge about the geometry of the open pore structure and about how it is affected by densification because nitrogen molecules cannot access the bulk of the cellulose as can water.[19]

In the pressure interval where adsorption on the cellulose structure occurs due to condensation in pores of successively larger diameters, the relation between the radius r of the pores being filled at a certain relative pressure can be expressed as[20]

$$r = -\frac{2\gamma V_{\mathrm{mol}}}{RT\ln(x)} = \frac{-9.5664 \times 10^{-8}\,\mathrm{cm}}{\ln(x)} \qquad (1)$$

for nitrogen adsorption.

Here, γ is the surface tension of the liquid condensate (8.85×10^{-7} J/cm^2 for nitrogen), V_{mol} is the molar volume (34.6 cm^3 at 77 K for nitrogen), and R is the molar gas constant (8.314 J/mol K). At high surface coverage, when capillary condensation dominates the adsorption process, the interface between the solid adsorber and the gas adsorbent is controlled by the liquid/gas surface tensions.[21] At the lower end of the adsorption isotherm, representing the early stages of multilayer build-up, the material/gas interface is controlled by attractive van der Waals forces between the gas and the solid material.[21]

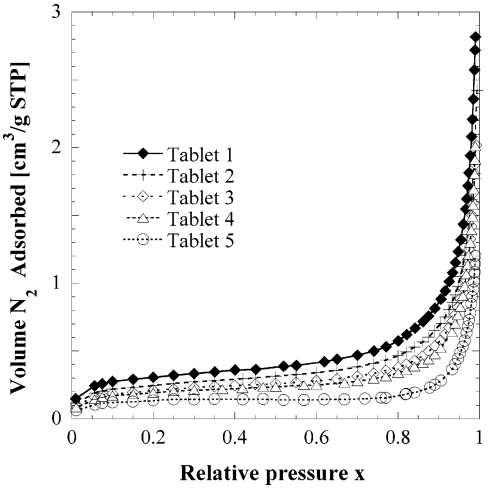

Figure 1. Nitrogen adsorption isotherms for the five different tablet batches, Table 1, of microcrystalline cellulose plotted vs partial nitrogen pressure.

The isotherm equation

$$N/N_{\mathrm{m}} \propto [\ln(1/x)]^S \qquad (2)$$

has been shown to describe adsorption in both the multilayer[21,22] and the capillary condensation[17,21] regime. In this equation, N_{m} is the number of molecules in a monolayer, and the exponent S equals $D - 3$ when liquid−gas interactions dominate the adsorption process, i.e., in the capillary condensation regime.[21] Here, D is the fractal dimension of the accessible surface of the investigated material. If, on the other hand, surface tension forces are negligible and instead the interactions at the interface are dominated by the van der Waals forces between the solid adsorber and the gas adsorbent, i.e., in the multilayer adsorption region, the exponent is $(D - 3)/3$.[21,22] For S values between −1 and 0, the dominant force can be roughly estimated from the equation[21]

$$\delta = 3(1 + S) - 2 \qquad (3)$$

If $\delta < 0$, the liquid−gas surface tension forces are dominant and $S + 3$ can be taken as a good estimate of the fractal surface dimension of the adsorber material. If instead $\delta > 0$, van der Waals forces dominate and $3(1 + S)$ is considered a reliable value of the fractal dimension.

Moisture Content. The equilibrium moisture content was measured gravimetrically after samples had been stored for one month at 22 °C over saturated salt solutions of NaI corresponding to 37% relative humidity (RH).[23] Prior to the measurements, the samples were stored over P_2O_5 (0% RH) for one month.

SEM. Scanning electron micrographs were taken (Phillips LEO 1550, Netherlands). The tablets were prepared by sputtering of a thin layer of gold−palladium (90−10%) onto their outer surface.

Results and Discussion

Nitrogen Adsorption Isotherms. Figure 1 shows the nitrogen adsorption isotherms for the different batches under study. No

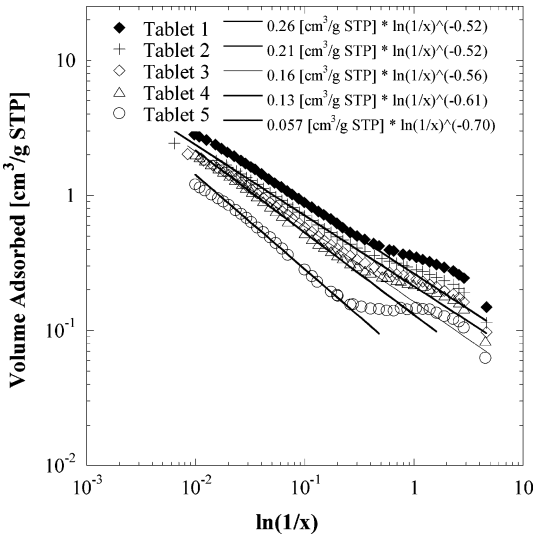

Figure 2. Nitrogen adsorption isotherms of Figure 1 shown vs the logarithm of the inverse partial nitrogen pressure on a log−log scale. Curve fits of eq 2 are included as solid lines, and the corresponding equations are displayed.

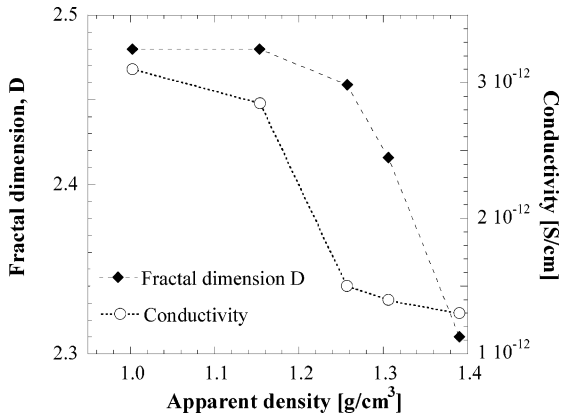

Figure 3. Fractal dimension *D*, extracted from the analysis in Figure 2, together with the ionic conductivity obtained from dielectric spectroscopy on MCC tablets at 37% RH.[6] The presented *D* values represent averages over 3 measurements and the variation in each data point is less than 8%, while the presented conductivity values are averages over ∼5 measurements and the variation in each data point is less than 25%.

leveling off of the volume adsorbed at high relative pressures was observed, and the isotherms could be essentially regarded as type II. Such isotherms usually have no or very narrow hysteresis between adsorption and desorption isotherms arising from V-shaped or conical pores.[24] From the figure, it is obvious that less nitrogen is adsorbed with higher tablet density. In Figure 2, the N_2 adsorption isotherms are plotted vs the logarithm of the inverse relative pressure in order to allow for an extraction of the fractal dimension using eq 2. It can be seen that the onset of the linear region, i.e., the region where this equation is applicable, is shifted toward higher relative pressures with increasing tablet density.

By performing a fit of eq 2 to the linear curve regions of Figure 2, a fractal dimension of the tablet surface, available to N_2 molecules, can be extracted. The fits are shown as solid lines and the exponents *S* lie in the −0.52 to −0.70 interval, indicating that the dominant interface forces can be attributed to the surface tension between the gas and the adsorbed liquid phase. The fractal dimension can thus be estimated as $S + 3$, and the observed shift in the onset of condensation from $\ln(1/x) \approx 0.47$ for Tablets 1 to $\ln(1/x) \approx 0.20$ for Tablets 5 should be a consequence of a decrease in the total volume of pores with

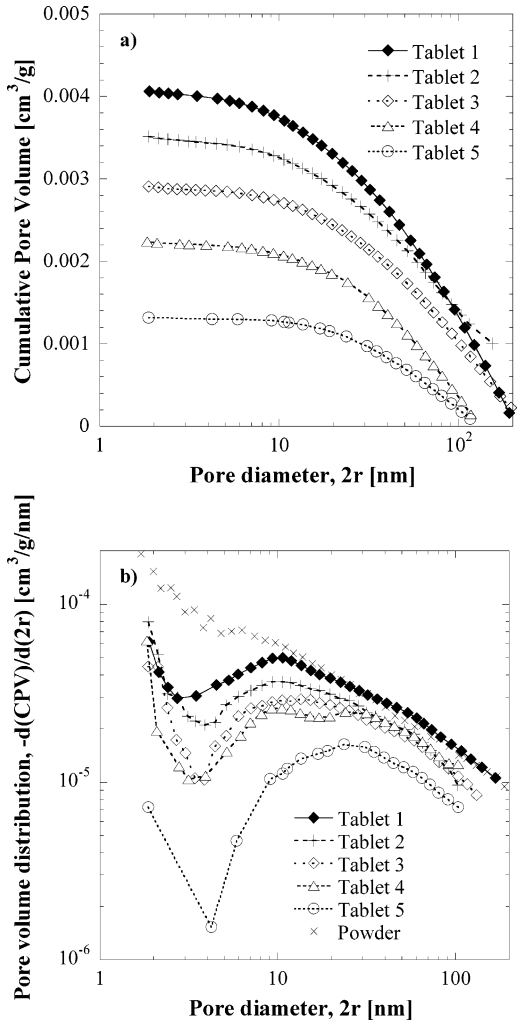

Figure 4. (a) Cumulative pore volume (CPV) and (b) pore volume distribution, respectively, vs pore diameter for the different tablet batches under study, as obtained from a BJH analysis of nitrogen adsorption isotherms. Included in panel (b) is also the pore volume distribution for uncompacted MCC powder as obtained from ref 19.

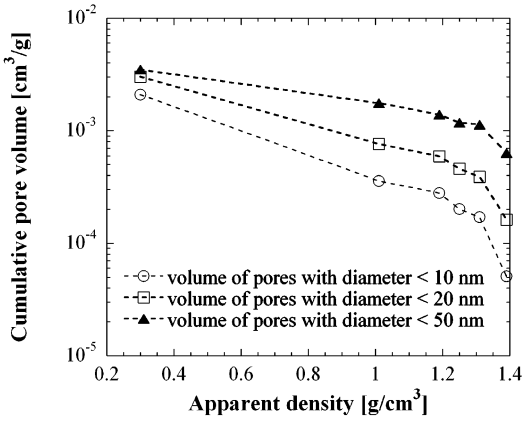

Figure 5. Volume of pores with a diameter smaller than 10, 20, and 50 nm, respectively, vs tablet density. The lowest density data point pertains to MCC powder analyzed in ref 19.

radii in the 2.0−4.8 nm region, according to eq 1, as the tablet density increases.

Fractal Dimension. Figure 3, displaying the extracted values of *D*, shows that the fractal dimension remains rather constant and ∼2.48 for the lowest tablet densities and starts to decrease at densities above 1.2 g/cm^3 to reach a value of ∼2.30 for the

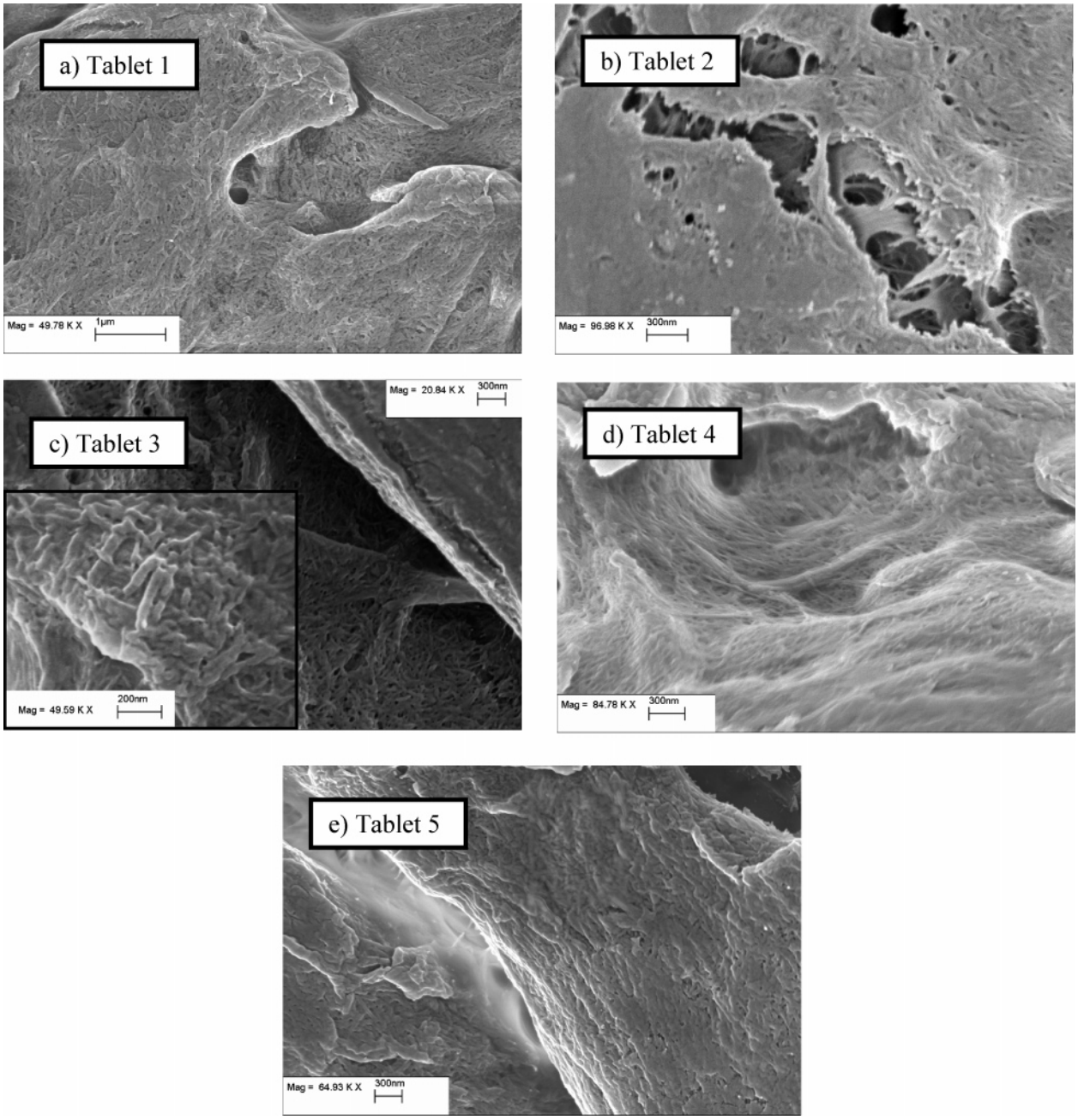

Figure 6. SEM micrographs of MCC tablets of different densities. The inset in panel (c) is a magnification of another part of the same tablet. The scaling bar has the length 300 nm in all panels except panel (a), where the length is 1 μm, and the inset in panel (c), where the length is 200 nm.

1.39 g/cm^3 tablets. By applying eq 2 to the nitrogen adsorption isotherms used for the fractal analysis performed in Strømme et al.[25] for uncompacted MCC (Avicel PH102) powder, the fractal dimension is also obtained as ∼2.48, supporting the above observation that D remains unaffected by the compaction process at low compaction pressures. The length scales probed by the present analysis is, according to eq 1 and the extent of the linear curve regions in Figure 2, from ∼2.0−4.8 nm to ∼50−100 nm.

The fractal dimension being nearly density-independent at low tablet densities indicates that compaction pressures below ∼200 MPa have little effect on the nanoscale roughness of the nitrogen accessible open pore surfaces in the MCC. At pressures above 200 MPa, however, structures smaller than ∼100 nm become smoother.

Included in Figure 3 are also the ionic conductivities previously obtained from dielectric spectroscopy[6] measurements on MCC tablets within the same density interval as those under present study and at a RH of 37% representing monolayer coverage humidity. From this figure, it can be observed that the earlier observed drop off in conductivity takes place at the same tablet density for which the fractal dimension starts to decrease.

Pore Structure. Figure 4a shows the cumulative pore volume (CPV) vs pore diameter for the different tablets, as obtained from the BJH analysis performed using the ASAP 2010. The pore volume distributions of the various tablets, in terms of the negative derivative of the CPV with respect to pore diameter, are displayed in Figure 4b. For comparison, this panel also includes the pore volume distribution for the uncompacted MCC powder, with a bulk density of ∼0.3 g/cm^3, analyzed in detail in ref 19. Several interesting features are visible in these plots.

First we observe that, when MCC powder is compacted, the shape of the pore volume distribution functions undergoes

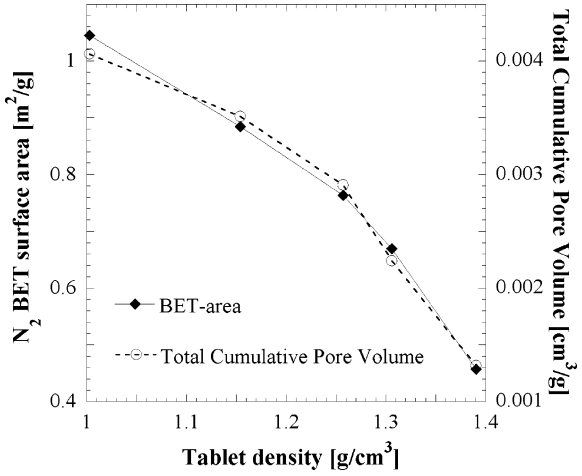

Figure 7. Surface area and total cumulative pore volume extracted from a BET and BJH analysis, respectively, of nitrogen adsorption isotherms are shown vs tablet density. The values are averages over 3 measurements and the variation in each data point is less than 3 and 5%, respectively.

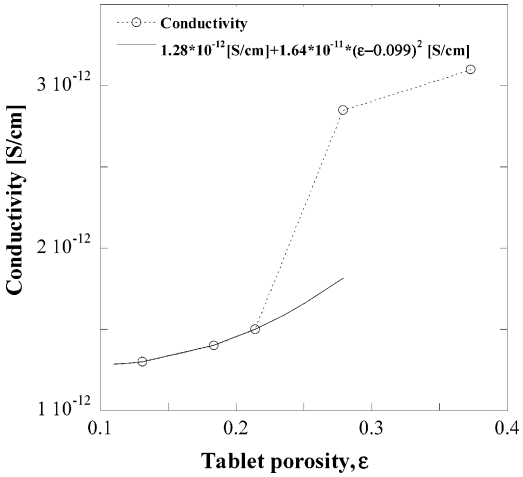

Figure 8. Conductivity from Figure 3 plotted vs tablet porosity. Included in the figure is a curve fit to eq 5 for the lowest porosity values. The equation describing the fit is also displayed.

significant changes for pores with diameters between ~5 and 50 nm. As the compaction pressure is increased beyond ~200 MPa, the peak broadens and appears to shift toward higher pore diameters along with the expected reduction in total measured pore volume. The shift in the peak position is clearly an effect of the compaction pressure reducing the total volume of small mesopores (~5−20 nm in diameter) to a larger extent than the macropore (above 50 nm in diameter) volume.

The change in mesopore volume can be studied in more detail in Figure 5, where the decreases in pore volume with increasing MCC density is shown for pore diameters smaller than 10, 20, and 50 nm, respectively. From this figure, it is obvious that the small mesopores are rapidly extinguished as the tablet density increases above ~1.3 g/cm^3. It is clear from this plot that smaller pores undergo much larger changes than the large ones. This observation is not surprising considering the fact that MCC undergoes excessive plastic deformation during tabletting. Hence, at very high compaction pressures, the contact surfaces are being flattened and smaller pore fractions present due to the irregularities of particle surfaces disappear.

Figure 6 shows SEM images of the cellulose tablet structures at length scales exceeding ~10 nm. The reduction in mesopore density can clearly be seen by comparing, e.g., the ~400 MPa compacted tablet in Figure 6e to the ~200 MPa compacted one in Figure 6c. An enlargement of the ~200 MPa tablet structure is shown in the inset of Figure 6c to visualize the individual cellulose fibril aggregates. From this image, one can extract rodlike structures with a width of ~40 nm, corresponding to fibril aggregates containing ~10 × 10 crystalline cellulose microfibrils. Thus, about 36% of the microfibrils in an aggregate are situated on the surface of open pores in the material.

Figure 7 shows the surface area available to nitrogen molecules vs tablet density as obtained by a BET analysis of the adsorption isotherms at relative pressures below 0.3. The total CPV extracted from data of the type presented in Figure 4a is also displayed in this panel. In contrast to the fractal dimension and the conductivity, the total surface area and pore volume accessible to nitrogen molecules decrease smoothly with increasing density over the entire density interval under study, showing that the overall amount of open surfaces steadily diminishes as the compaction pressure increases.

Percolation of Mesopore Network. The average moisture content of the cellulose samples at 37% RH was 0.044 g water/g cellulose. It has previously been reported that moisture sorption isotherms on powdered MCC[19] is close to identical to isotherms measured on compacted MCC powder.[26] This is because water is being sorbed *both* into the open pore structure *and* into amorphous regions of the cellulose bulk.[19] Even if the open pore volume is reduced during compaction, the amorphicity of the initially open surfaces is preserved, allowing for the same amount of water molecules to reside in the structures of varying densities. This shows that the background of the rapid decrease in conductivity, Figure 3, for tablets compacted at pressures above ~200 MPa, is most likely caused by a decrease in ion mobility because the number of charge carriers and sites available for water-induced conduction do not change.

As mentioned above, the conductivity depicted in Figure 3 is probably governed by impurity ions, such as Na^+, and protons or H_3O^+ ions jumping between neighboring OH^- groups in disordered regions of the cellulose to which a water molecule is attached.[7] Interpreting this ionic charge transport process from a percolation theory perspective,[27−29] the cellulose host can be viewed as a system consisting of nonconducting crystalline regions and conducting amorphous regions. The amorphous regions can either be situated in the bulk of the cellulose material or be associated with surfaces of open pores.[18,25] To clearly visualize how the charge transport process varies with the cellulose porosity, the conductivity is plotted vs tablet porosity ϵ instead of density ρ in Figure 8. The porosity is obtained as

$$\epsilon = \frac{\rho_{\max} - \rho}{\rho_{\max}} \tag{4}$$

where $\rho_{\max}$ is the true density of MCC previously determined to ~1.6 g/cm^3.[30,31]

According to percolation theory and from random resistor simulations of three-dimensional systems, the conductivity σ of the MCC tablets under present study can be expressed by[32,33]

$$\sigma = \sigma_{\text{bulk}} + \sigma_0(\epsilon - \epsilon_c)^2 \tag{5}$$

in a region where $\epsilon - \epsilon_c \leq \sim 0.2$. Here, σ_{bulk} denotes the conductivity of the tablets at zero porosity, σ_0 is a constant proportional to the conductivity on the open pore surfaces, and ϵ_c signifies the threshold porosity at which the first path of open pore surface sites cross through the entire tablet matrix. Fitting eq 5 to Figure 8 gives an ϵ_c of ~0.1. This shows that, even for the densest tablets under study ($\rho \approx 1.4$ g/cm^3, $\epsilon \approx 0.13$),

continuous open pore structures exist through which ion conduction can proceed. However, it is not until ϵ reaches a value of $\geq\sim0.25$ ($\rho \leq \sim1.2$ g/cm^3) that the conduction on open pore surfaces starts to dominate over the conduction process taking place within the amorphous bulk. Relating this result to the pore structure data of Figures 4 and 5, it is obvious that the mesopore network plays a dominant role in the water-induced charge transport of compacted MCC even if the sites available for primary water bindings on the surfaces of these pores only constitute ~36% of the total number of sites available for primary water bindings on all microfibril surfaces. Decreasing the tablet density below ~1.2 g/cm^3 results in a significant increase of pores with a diameter between ~5 and 20 nm. This indicates that the critical pore channel width, distinguishing the amorphous bulk regions from the open pore surfaces acting as water-induced ionic transport paths, lies in this interval. When the network of pores with a diameter in this interval is reduced to the point where it no longer forms a continuous passageway throughout the compact, the conduction process is dominated by the transport in amorphous regions of the cellulose bulk, i.e., on the surfaces of individual microfibrils mainly situated in the bulk of the fibril aggregates. The conductivity of this process is of the order of 1×10^{-12} S/cm at 37% RH, cf. Figure 8. Sufficiently above the percolation threshold where a continuous mesopore network is formed, the conductivity increases to a ~200% higher value and the dependence of the conductivity on porosity levels out.

Summary and Conclusion

Nitrogen adsorption isotherms as well as SEM micrographs of MCC tablets formed at different compaction pressures were analyzed to obtain information about tablet pore structure, surface area, and fractal dimension of internal pore surfaces. The results of this analysis were compared to the ionic charge transport properties of the cellulose tablets.

The fractal analysis of nitrogen adsorption isotherms showed that the dominant interface forces during adsorption could be attributed to the surface tension between the gas and the adsorbed liquid phase. The fractal dimension, characterizing the pore surfaces of the tablets in the length scale region from ~2.0−4.8 nm to ~50−100 nm, was shown to decrease from a constant value of ~2.5 for tablets of densities lower than ~1.2 g/cm^3 to ~2.3 for tablets with a density of ~1.4 g/cm^3. This decrease of surface fractality coincided with a rapid reduction of mesopore volume and a decrease in the water-induced ionic conductivity.

The ionic conductivity at 37% RH, previously shown to be governed by impurity ions and/or protons jumping between neighboring water molecules bound to OH^- groups on the amorphous microfibril surfaces, was analyzed in terms of a percolation model. The analysis showed that a nonporous MCC at 37% RH transports ions at a conductivity of the order of 1×10^{-12} S/cm, while opening up the mesopore structure leads to an increase of ~200% in the conductivity. The porosity percolation threshold for this facilitated conduction was shown to be ~0.1. However, it is not until ϵ reaches a value of $\geq\sim0.25$ ($\rho \leq \sim1.2$ g/cm^3) that the conduction on open mesopore surfaces starts to dominate over the conduction process taking place within the amorphous bulk. Deduced from the size of the cellulose fibril aggregates visible in SEM micrographs, these surfaces constitute ~36% of the total amount of microfibril surfaces available for water-induced ionic transport.

The above findings emphasize the importance of analyzing and being able to control the mesopore structure of a pharmaceutical cellulose-based system in order to tailor the drug transport properties related to cellulose−water interactions. The results presented in this study should also be significant to other fields where cellulose−water interactions are a key issue such as for paper and sanitary product research and for food industries using cellulose-based gels.

Acknowledgment. M.S. is a Royal Swedish Academy of Sciences (KVA) Research Fellow and thanks the Academy for their support. The Swedish Foundation for Strategic Research (SSF) is also acknowledged for their support to our multidisciplinary research in materials physics and pharmaceutics.

References and Notes

(1) Israelachvili, J. *Intermolecular and Surface Forces*, 2nd ed.; Academic Press: London, 1992.
(2) Brohede, U.; Frenning, G.; Strømme, M. *J. Pharm. Sci.* **2004**, *93*, 1796.
(3) Gustafsson, C.; Lennholm, H.; Iversen, T.; Nyström, C. *Drug Dev. Ind. Pharm.* **2003**, *29*, 1095.
(4) Larsson, P. T.; Wickholm, K.; Iversen, T. *Carbohydr. Res.* **1997**, *302*, 19.
(5) Wickholm, K.; Larsson, P. T.; Iversen, T. *Carbohydr. Res.* **1998**, *312*, 123.
(6) Nilsson, M.; Alderborn, G.; Strømme, M. *Chem. Phys.* **2003**, *295*, 159.
(7) Nilsson, M.; Strømme, M. *J. Phys. Chem. B* **2005**, *109*, 5450.
(8) Murphy, E. J. *J. Phys. Chem. Solids* **1960**, *16*, 115.
(9) Pethig, R. *Dielectric and Electronic Properties of Biological Materials*; Wiley: Chichester, UK, 1979.
(10) Sapieha, S.; Inoue, M.; Lepoutre, P. *J. Appl. Poym. Sci.* **1985**, *30*, 1257.
(11) Simula, S.; Niskanen, K. *Nord. Pulp Pap. Res. J.* **1999**, *14*, 243.
(12) Zografi, G.; Kontny, M. J.; Yang, A. Y. S.; Brenner, G. S. *Int. J. Pharm.* **1984,** *18*, *99*.
(13) Ardizzone, S.; Dioguardi, F. S.; Mussini, T.; Mussini, P. R.; Rondini, S.; Vercelli, B.; Vertova, A. *Cellulose* **1999**, *6*, 57.
(14) Brunauer, S.; Emmet, P. H.; Teller, E. *J. Am. Chem. Soc.* **1938**, *60*, 309.
(15) Barret, E. P.; Joyner, L. G.; Halenda, P. P. *J. Am. Chem. Soc.* **1951**, *73*, 373.
(16) Pfeifer, P.; Obert, M.; Cole, M. W. *Proc. R. Soc. London, Ser. A* **1989**, *423*, 169.
(17) Yin, Y. *Langmuir* **1991**, *7*, 216.
(18) Mihranyan, A., Strømme, M. *Chem. Phys. Lett.* **2004**, *393*, 389.
(19) Mihranyan, A.; Llagostera, A. P.; Karmhag, R.; Strømme, M.; Ek, R. *Int. J. Pharm.* **2004**, *269*, 433.
(20) Kelvin, J. *Philos. Mag.* **1871**, *42*, 448, published under the name of Sir William Thomson.
(21) Ismail, I. M. K.; Pfeifer, P. *Langmuir* **1994**, *10*, 1532.
(22) Pfeifer, P.; Wu, Y. J.; Cole, M. W.; Krim, J. *Phys. Rev. Lett.* **1989**, *62*, 1997.
(23) Nyqvist, H. *Int. J. Pharm. Technol. Prod. Manuf.* **1983**, *4* (2), 47.
(24) Sing, K. S. W.; Everett, D. H.; Haul, R. A. W.; Moscou, L.; Pierotti, R. A.; Rouquerol, J.; Siemieniewska, T. *Pure Appl. Chem.* **1985**, *57*, 603.
(25) Strømme, M.; Mihranyan, A.; Ek, R.; Niklasson, G. A. *J. Phys. Chem. B* **2003**, *107*, 14378.
(26) Khan, F.; Pilpel, N. *Powder Technol.* **1987**, *50*, 237.
(27) Deutscher, G.; Kapitulnik, A.; Rappaport, M. *Percolation, Structures, and Processes* Ayalon, Offset: Haifa, Israel, 1983.
(28) Stauffer, D.; Aharony, A. *Introduction to Percolation Theory*, 2nd ed.; Taylor & Francis: London, UK, 1992.
(29) Sahimi, M. *Applications of percolation theory*, Taylor & Francis: London, UK, 1994.
(30) Zhang, Y.; Law, Y.; Chakrabarti, S. *AAPS PharmSciTech.* **2003**, *4*, article 62.
(31) Schmidt, C.; Leinebudde, P. K. *Chem. Pharm. Bull.* **1999**, *47*, 405.
(32) Kirkpatrick, S. *Rev. Mod. Phys.* **1973**, *45*, 574.
(33) Gingold, D. B.; Lobb, C. J. *Phys. Rev. B* **1990**, *42*, 8220.